HCN Channel Activity Balances Quiescence and Proliferation in Neural Stem Cells and Is a Selective Target for Neuroprotection During Cancer Treatment

Helena Johard[1,2,3], Anna Omelyanenko[1], Gao Fei[1,4], Misha Zilberter[5], Zankruti Dave[2], Randa Abu-Youssef[1], Linnéa Schmidt[2], Aditya Harisankar[6], C. Theresa Vincent[2,7], Julian Walfridsson[6], Sven Nelander[2], Tibor Harkany[8,9], Klas Blomgren[10,11], and Michael Andäng[1,2,3]

ABSTRACT

Children suffering from neurologic cancers undergoing chemotherapy and radiotherapy are at high risk of reduced neurocognitive abilities likely via damage to proliferating neural stem cells (NSC). Therefore, strategies to protect NSCs are needed. We argue that induced cell-cycle arrest/quiescence in NSCs during cancer treatment can represent such a strategy. Here, we show that hyperpolarization-activated cyclic nucleotide-gated (HCN) ion channels are dynamically expressed over the cell cycle in NSCs, depolarize the membrane potential, underlie spontaneous calcium oscillations and are required to maintain NSCs in the actively proliferating pool. Hyperpolarizing pharmacologic inhibition of HCN channels during exposure to ionizing radiation protects NSCs cells in neurogenic brain regions of young mice. In contrast, brain tumor–initiating cells, which also express HCN channels, remain proliferative during HCN inhibition.

Implications: Our finding that NSCs can be selectively rescued while cancer cells remain sensitive to the treatment, provide a foundation for reduction of cognitive impairment in children with neurologic cancers.

Introduction

Even though neurologic childhood cancers have increased over the past 20 years, the survival rates have also greatly improved (1). Unfortunately, both chemotherapy and radiotherapy pose well-known risks of inducing neurocognitive damage with severe impact on these young children's quality of life and requiring extensive posttreatment cognitive rehabilitation therapy (2). It is likely that these side effects on cognitive development stem from damage to the proliferating neural stem cell (NSC) pool, as postnatal neurogenesis regulates critical functions such as learning and memory (3, 4). The production of neurons by the NSCs continues at a reduced rate throughout life in the subgranular zone of the hippocampus (SGZ) and in the subventricular zone along the lateral ventricles (SVZ; refs. 5–7). To develop new therapeutic strategies protecting against damage during cancer treatments a deeper understanding of the regulatory mechanisms controlling NSC proliferation is needed. So far, strategies to rescue neurogenesis have focused on reactivating and increasing NSC proliferation after radiotherapy (8–10). Another strategy is to selectively induce quiescence while maintaining cancer cells in a proliferative state. Such a strategy has not been reported yet and requires deeper understanding of control mechanisms that diverge in normal and transformed cells.

Proliferation of NSCs as well as cancer cells is maintained by a variety of extracellular signals in the microenvironment (11–13) including signaling via neurotransmitters that control the membrane potential. For example, chloride-permeable $GABA_A$ receptor channels limit proliferation via hyperpolarization, while glutamate receptors activate proliferation via depolarization (14). Interestingly, highly proliferating cancer cells are thought to have a more depolarized membrane potential conductive toward sustained proliferation in comparison with nonmalignant cells (15). This suggests a divergence in maintenance of membrane potential in malignant cells likely via altered expression of ion channels.

Here we explore HCN ion channels as putative target for proliferative control in NSCs. HCN channels have neither previously been investigated in NSCs nor in cancer cells, although HCN expression has been linked to proliferation in embryonic stem cells (16, 17). The HCN channel family consists of 4 isoforms (HCN1–4) and conduct potassium and sodium, with HCN2 being also slightly permeable to calcium (18). In response to membrane hyperpolarization in excitable cells, HCN channels conduct a depolarizing current, referred to as h-current (I_h),contributing toward an electric feedback loop essential for pace-making cyclic behavior in, for example, cardiac pacemaker cells of the heart (19) and neuronal oscillations (20), including circadian rhythmicity in the suprachiasmatic nucleus (21, 22).

We show that HCN channel activity is critical for maintaining NSCs in the actively proliferating pool. Hyperpolarization by pharmacologic

[1]Department of Physiology and Pharmacology, Karolinska Institutet, Stockholm, Sweden. [2]Department of Immunology, Genetics and Pathology, Uppsala University, Rudbeck Laboratory, Uppsala, Sweden. [3]Central European Institute of Technology, Masaryk University, Brno, Czech Republic. [4]College of Veterinary Medicine, Jilin University, Changchun, Jilin, China. [5]Gladstone Institute of Neurological Disease, San Francisco, California. [6]Department of Medicine, Karolinska Institutet, Huddinge, Sweden. [7]Department of Microbiology, New York University School of Medicine, New York, New York. [8]Department of Neuroscience, Karolinska Institutet, Solna, Sweden. [9]Department of Molecular Neurosciences, Center for Brain Research, Medical University of Vienna, Vienna, Austria. [10]Department of Women's and Children's Health, Karolinska Institutet, Stockholm, Sweden. [11]Pediatric Oncology, Karolinska University Hospital, Stockholm, Sweden.

Note: Supplementary data for this article are available at Molecular Cancer Research Online (http://mcr.aacrjournals.org/).

H. Johard, A. Omelyanenko, and G. Fei contributed equally to this article.

Corresponding Author: Michael Andäng, Uppsala University, Rudbeck Laboratory, Uppsala 751 85, Sweden. Phone: 467-0331-4682; E-mail: michael.andang@igp.uu.se

Mol Cancer Res 2020;18:1522–33

doi: 10.1158/1541-7786.MCR-20-0292

inhibition of HCN channels induces quiescence in NSCs, while leaving brain tumor cells unaffected. This selective effect protects NSCs from genotoxic insult *in vivo* and thereby constitutes a novel approach for neuroprotection during cancer treatment by directly reducing damage to NSCs.

Materials and Methods

Animals

Mouse strains used to generate *in vitro* cultures were GFAP::GFP reporter mice (23). *In vivo* drug action experiments were performed on wild-type C57/B6 animals. Ethical permissions were obtained for all animal work (permit number N397/12, N 248-13, N 163-15). Work was carried out in accordance with rules and regulations governing animal research in Sweden.

Neurosphere derivation and generation of NSC lines

Neurosphere cultures were prepared as described previously (24). NSCs isolated from sphere cultures were further cultured in monolayer as described previously (25).

Electrophysiology

Whole-cell patch clamp recordings were performed on selected cells in voltage-clamp mode, recorded, and digitized at 10 kHz with EPC10 amplifier and digitizer (HEKA). The composition of the intracellular solution was 140 mmol/L $CsMeSO_4$, 10 mmol/L HEPES, 2 mmol/L $MgCl_2$, 0.6 mmol/L EGTA, 2 mmol/L ATPNa, 0.3 mmol/L GTPNa, set to pH 7.2–7.3 with CsOH, osmolarity 270 –280 mOsm. The composition of the extracellular solution ACSF was 124 mmol/L NaCl, 30 mmol/L $NaHCO_3$, 10 mmol/L glucose, 1.25 mmol/L NaH_2PO_4, 3.5 mmol/L KCl, 1.5 mmol/L $MgCl_2$, 1.5 mmol/L $CaCl_2$. HCN positivity was ascertained as a presence of a slow-activating inward current at a 5-second step to -110 mV. Resting membrane potential (E_m) was calculated from voltage–current relationships (I–V curves) recorded from a series of voltage steps from -100 to +30 mV in 10-mV increments.

Live-cell calcium imaging

Cells were cultured in 35-mm Petri dishes until approximately 70% confluence, after which half of their medium was removed and dishes were loaded with 10 μmol/L Ca^{2+}-sensitive indicator [either Fluo-4 (Invitrogen, P3000MP), Fluo-8 (Teflabs, 0203), or Fura-2 (Life Technologies, F1221)] for 30 minutes in a 37°C humidified incubator. Dishes were subsequently washed with phenol-free DMEM/F-12 (Gibco, 21041-025). Ca^{2+} recordings were performed in this phenol red–free DMEM at 37 °C by means of a heat-controlled chamber (QE-1; Warner Instruments) with a cooled electron-multiplying charged-coupled device Cascade II:512 camera (Photometrics) mounted on an inverted microscope (Zeiss Axiovert 100M; Carl Zeiss) equipped with an 25 × 0.8 N.A. lens (Carl Zeiss). Excitation was at 488 nm (Fluo-4 and Fluo-8) or at 340/380 nm (Fura-2) with a Lambda LS xenon-arc lamp equipped with a SmartShutter (Sutter Instrument) at snapshot frequency of every second or other second. After establish baseline oscillatory activity for approximately 15 minutes, ZD7288 (10 μmol/L) was applied. Recordings were analyzed by MetaFluor software (Molecular Devices). ROI actively oscillating before drug application through were selected and quantitative fluorescence data per time interval was logged in an Excel spreadsheet, after which graphical representation of intracellular calcium oscillations was created with GraphPad Prism 6 (GraphPad Software, Inc.).

Flow cytometry

For cell-cycle profile analyses, DNA profiles were acquired with BD CellQuest Pro software, and percentages of G_1, S, and G_2 phases were calculated and graphically presented with MODFIT software. For cell-cycle sorting, adherent NSCs were incubated in darkness for 30 minutes in the presence of Hoechst 33258 (10 μg/mL, Sigma-Aldrich). Cells were trypsinized and resuspended in 37°C conditioned Hoechst media and sorted for DNA content on a FACSVantage SE (Becton Dickinson) at 4°C and cell-cycle fractions corresponding to G_1–G_0, S, and G_2–M were collected in conditioned media on ice.

Cell cycle sorting of cells for electrophysiological recordings was also done by transfecting cells with Gem-AG (26) plasmid obtained from the RIKEN BioResource Research Center DNA Bank.

Assays used for viable cell counting

ATP-based cell number assays were used after treatment as described previously (27). The following chemical compounds used in cell-based assays: ZD7288 (Tocris Bioscience), Zatebradine (Tocris Bioscience), CsCl (Sigma), and SR9009 (Calbiochem).

Gene expression analysis and statistics

RNA was isolated using the RNeasy Micro Kit (Qiagen). For qRT-PCR, 1 μg of RNA was reverse transcribed using the High Capacity cDNA Reverse Transcription Kit (Applied Biosystems). Transcript abundance was assayed with qRT-PCR using gene-specific primer pairs and SYBR reagents (Invitrogen) with a 7500 Fast Real-Time PCR machine (Applied Biosystems).

Primer sequences

Hcn1 Forward: 5′CGC CTT TCA AGG TTA ATC AGA 3′
Hcn1 Reverse: 5′ GGC GAG GTC ATA GGT CAT GT 3′
Hcn2 Forward: 5′ GCT CAT CCG ATA TAT CCA CCA 3′
Hcn2 Reverse: 5′ CTT GCC AGG TCG TAG GTC AT 3′
Hcn3 Forward: 5′ CCT CAT CCG CTA CAT ACA CCA 3′
Hcn3 Reverse: 5′ ACT GGC CAG GTC GTA GGT C 3′
Hcn4 Forward: 5′ CCA TCA ATG GCA TGG TGA 3′
Hcn4 Reverse: 5′ CCT TGA AGA GGG CGT AGG A 3′

For RNA sequencing, RNA quality was verified with the RNA Nano Chip (Agilent Technologies) on the Bioanalyzer 2100 (Agilent). Three-hundred nanograms of total RNA per sample was used to generate a sequencing library using the TrueSeq Stranded RNA LT Kit (Illumina), as per manufacturer's instructions. Samples were sequenced on an Illumina HiSeq 2000 sequencer as single-end 51-nucleotide reads according to the manufacturer's protocol. Raw reads were mapped to the reference human genome and normalized data was generated for each genomic feature using STRT software (28). Briefly, raw reads were aligned using Bowtie (29). Mapped reads were normalized using reads per kb per million reads (RPKM) normalization method (30), whereas unmapped reads were removed. Analysis of RNA-sequencing data was done using DAVID (http://david.abcc.ncifcrf.gov) and GeneVenn (http://genevenn.sourceforge.net).

shRNA transduction and gene knockdown

shRNA plasmids were designed according to a previously published protocol (31). Targeting sequences used were CGGCTCATCCGATATATCCACC for Hcn2 and GCAGTACATGTCCTTCCACAAG for Hcn3. Constructs were cloned into the previously described pInducer system (32). shRNA was delivered via lentiviral transduction.

Lentiviral particles were produced by calcium phosphate–based transfections by mixing 8 μg of the packaging plasmid, pCMV-dR8.74psPAX2, and 4 μg of the VSV-G envelope plasmid along with 10 μg of the shRNA-expressing plasmid. The plasmid mixture was added to a solution of 2 mol/L $CaCl_2$ and mixed drop-wise into a HEPES (1×) buffer solution. The mix was incubated at room temperature for 10 minutes and then added to 293FT cells drop-wise. The following day, transfection medium was replaced with fresh medium and the lentiviral particles were collected at 24 and 48 hours post-transfection. The collected lentiviral particles were filtered through a 0.45-μm low protein-binding filter (TPP) to remove cellular debris. Next, the virus supernatant was spun overnight at 4,000 × *g* at 4°C to concentrate the lentiviral particles. NSCs at 70% confluence were transduced with the pooled and concentrated viral particles. Polybrene (4 μg/mL, Sigma) was added to the cells to increase transduction efficiency. Following 24 hours of transduction, the medium was replaced with fresh medium and the transduced cells were propagated for 48 hours to fully express their selection markers. Selection of transduced cells was performed by addition of puromycin (1 μg/mL, Life Technologies) for 5 days. shRNA expression was induced by adding 2 μg/mL doxycycline to culture media for 48 hours.

Immunostaining of cells in culture and Western blot analysis

Immunostainings and Western blotting were carried out as described previously (27). Immunostainings were analyzed using confocal microscopy (LSM710, Zeiss) and flow cytometry (CyAn ADP, Beckman Coulter). Data were analyzed using FlowJo software.

Staining of tissue sections

Immunostainings, Nissl, and DAB stainings, were done as described previously (33). Image analyses for cell counting in brain sections were performed by an observer blinded to the treatment of the animals. Cell counting was performed using stereologic principles on serial sagittal sections (Stereoinvestigator, MicroBrightField), 4–7 animals per group. $BrdU^+$, $Ki67^+$, and caspase-3^+ cells were counted in the SVZ and the SGZ of the hippocampus. The total number of cells was counted on each section. The total number of cells was obtained by multiplying the number of cells by the sampling fraction. Cell counts were analyzed using two-way ANOVA with treatment and age as main factors, and $P < 0.05$ was considered statistically significant. The antibodies used were: rabbit and mouse anti-SOX2, rabbit anti-Cyclin D, mouse anti-β-Actin, rabbit anti-EGFR, mouse anti-EGFR, rabbit anti-phospho-Histone 3, goat anti-GFAP, rabbit anti-γH2AX (from Abcam), rabbit anti-active caspase-3 (Abcam, BD Biosciences), rabbit anti-Ki-67 (Thermo Fisher Scientific, Leica Biosystems), rabbit anti-HCN2 and HCN3 (Alomone labs), rabbit anti-GFAP (Dako), rat anti-BrdU (Abcam, AbD Serotec), donkey anti-rat IgG BT (Jackson Immunoresearch Laboratories Inc.), Alexa Fluor–conjugated goat and donkey antibodies (Invitrogen).

Glioma tumor-initiating cells

Glioma-initiating cells (GIC) were obtained from the Uppsala University Human Glioma Cell Culture (HGCC) collection (34) and cultured as described previously (27, 35). Effects of ZD7288 on adherent human GIC cultures were screened as described previously (27).

Irradiation

A linear accelerator (Varian Clinac 600 CD, Radiation Oncology Systems LLC) with 4 MV nominal photon energy and a dose rate of 2.3 Gy/minute was used to irradiate mice on P12 as described previously (36).

Statistical analysis

Statistical calculations of Student *t* test and SEM were performed using GraphPad Prism v6.0. Significance levels were specified as *, $P < 0.05$; **, $P < 0.01$; ***, $P < 0.001$.

Results

HCN2 and HCN3 ion channel isoforms are expressed in proliferating NSCs

To identify ion channels that may have an impact on cell proliferation in NSCs, we mined the microarray mRNA expression data from Codega and colleagues (37) comparing actively proliferating (aNSC) versus quiescent (qNSC) NSCs, isolated from mouse brains. The analysis identified several ion channel genes, for example, $GABA_A$ receptor genes, as selectively expressed in qNSCs, while only two channel genes were selectively expressed in aNSCs (**Fig. 1A**), one of them being the voltage gated *Hcn3* channel. HCN channels are expressed in neurons throughout the CNS (38), but a role for HCN channels has not previously been described in NSCs and therefore this selective expression in the aNSC pool prompted further investigations.

To probe HCN expression in neural stem and progenitor cells (NSPC), neurospheres were prepared from the SVZ of mouse brain (**Fig. 1B**) and gene expression of *Hcn* channel isoforms was assessed by qRT-PCR. Both *Hcn2* and *Hcn3* genes were expressed in the NSPCs, with *Hcn2* expressed at higher levels than *Hcn3* (**Fig. 1C**). To further study HCN channel expression in NSPCs and more specifically in NSCs, neurospheres derived from the SVZ of adult mice expressing GFP from a human GFAP promoter fragment (GFAP::GFP) were prepared. To this end, GFP^{high} NSCs and GFP^{weak} progenitor cells (39) were separated by flow cytometry and Hcn mRNA expression was analyzed by qRT-PCR. Interestingly, both *Hcn2* and *Hcn3* were expressed in both populations (**Fig. 1D**), suggesting ubiquitous Hcn expression in proliferating cells in the SVZ niche.

We next analyzed HCN2 and HCN3 protein expression *in vivo* in the SVZ and SGZ regions of the mouse brain. Proliferating cells were labeled by administration of BrdU to mice prior to sacrifice and brain sections were immunostained for BrdU, HCN2, or HCN3 in combination with the NSC markers SOX2 or GFAP. Both HCN2/SOX2/BrdU and HCN3/SOX2/BrdU triple positive cells were found in the SVZ and SGZ (**Fig. 1E–G**), and triple positive cells stained for HCN3/SOX2/GFAP were identified within the SGZ (**Fig. 1H**). We concluded that HCN ion channels are expressed in proliferating cells, including NSCs, in both the SVZ and SGZ.

HCN channels are differentially expressed over the cell cycle with channel function restricted to the S-G_2–M phases

To investigate whether HCN channels are electrically active in NSCs, we performed whole-cell patch-clamp recordings in primary neurospheres derived from the SVZ. Under voltage-clamp conditions, a slow inward current developed during a -110 mV step (seen as downward deflection in the holding current), verifying the presence of an HCN-mediated hyperpolarization-activated depolarizing current (I_h). The current could be blocked using an I_h inhibitor (ZD7288, selective for I_h at 10 μmol/L; **Fig. 2A**). Stepwise increased voltages confirmed that the currents were activated by hyperpolarized potentials as expected for HCN-mediated currents (**Fig. 2B**).

To demonstrate a role between HCN channel activity and cell proliferation, neurospheres were transferred to adherent growth (25)

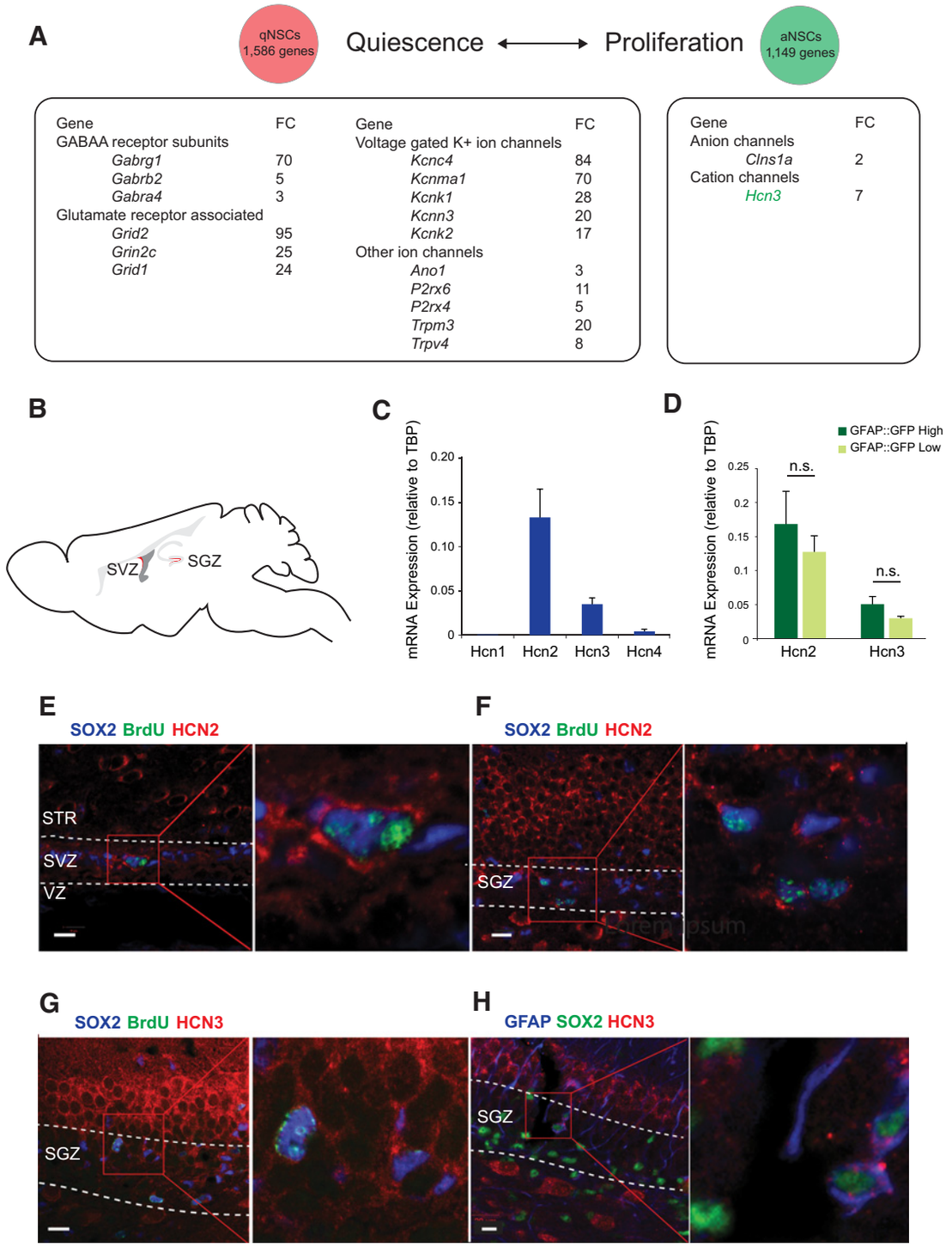

Figure 1.

HCN2 and HCN3 are expressed in proliferating NSCs. **A,** Data mining of gene enrichment set from Codega and colleagues (37) indicating differentially expressed ion channel genes in aNSCs versus qNSCs in the adult mouse SVZ region. **B–D,** Expression of HCN channels was analyzed in neurogenic SVZ and SGZ regions by qRT-PCR of Hcn channel mRNA in adult mouse SVZ-derived primary neurospheres (**C**) and neurospheres from TgN-GFAP::GFP mice sorted by flow cytometry based on GFP intensity ($n = 3$, Student t test; n.s. = not significant; **D**). **E–H,** Confocal images of neurogenic regions in sagittal brain sections of SVZ and SGZ [STR (striatum) and VZ (ventricular zone)]. **E** and **F,** Immunostaing for HCN2 (red), BrdU (green) and SOX2 (blue) in SVZ (**E**) and SGZ (**F**). Immunostaining for HCN3 (red) in SGZ colocalizing with BrdU (green) and SOX2 (blue; **G**) or BrdU (green) and GFAP (blue; **H**). Scale bars, 10 μm.

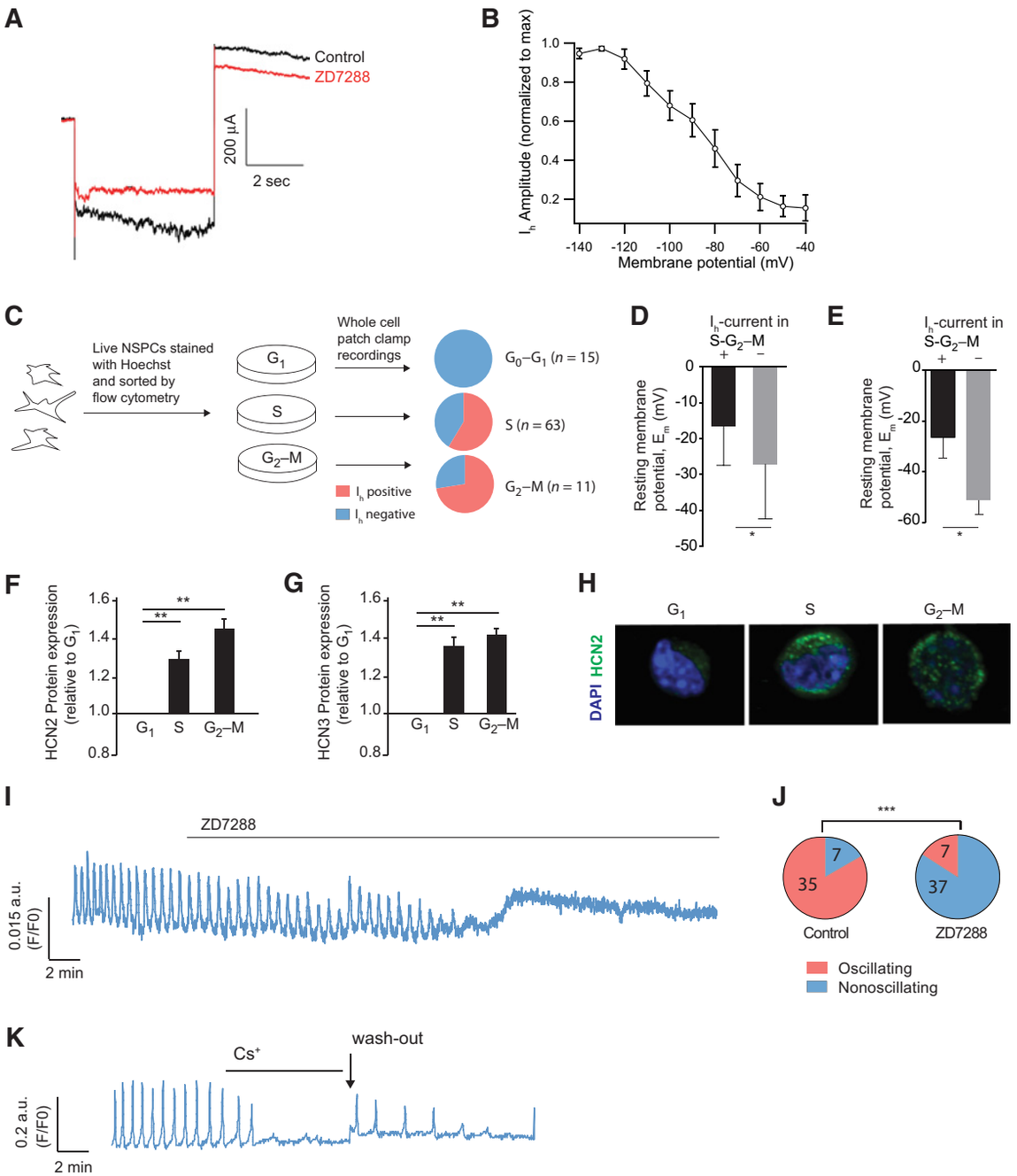

Figure 2.

HCN channel function is cell-cycle–dependent and correlates with a depolarized membrane potential and sustained spontaneous Ca^{2+} oscillations. **A,** Whole-cell patch clamp recordings of h-current at -110 mV in neurosphere NSCs before and after administration of 10 µmol/L ZD7288. **B,** Hyperpolarization-dependent activation was determined by I/V plot of currents under varying membrane potential (Mean I_h values, $n = 8$). **C,** After sorting adherently grown NSCs according to DNA content, I_h currents were recorded and found exclusively in S-G_2–M phases ($n = 89$ cells). **D,** Comparison of resting membrane potentials (E_m) in S-G_2–M sorted NSCs that had ($n = 18$ cells) or lacked ($n = 26$ cells) I_h. **E,** Comparison of resting membrane potentials (E_m) in Gem-AG^+ NSCs from primary neurospheres that had ($n = 2$ cells) or lacked ($n = 3$ cells) I_h. Expression of HCN2 (**F**) and HCN3 protein over the cell-cycle quantified in adherent NSCs by immunostaining and flow cytometry (normalized to G_1–G_0; **G**). HCN2 and HCN3 were expressed at higher levels in S-G_2–M phases as compared with G_1–G_0 phases ($n = 3$, ***, $P < 0.001$; **, $P \leq 0.01$, Student t test). **H,** Confocal image of cell-cycle–sorted NSCs immunostained with HCN2 antibody showed differences in HCN2 channel intensity and localization between phases (HCN2 green, DAPI blue). **I,** Spontaneous calcium oscillations recorded in NSCs during the administration of 10 µmol/L ZD7288 or vehicle. **J,** Pie chart showing number and proportion of NSCs exhibiting spontaneous calcium oscillations after vehicle versus application of 10 µmol/L ZD7288 (χ^2; ***, $P \leq 0.001$). While 83% of oscillating cells continued to oscillate 15 minutes after vehicle, only 16% of cells oscillated after administration of ZD7288. **K,** Spontaneous calcium oscillations recorded in NSCs during administration of Cs^+ at indicated time point followed by Cs^+ wash-out.

and adherent NSCs were labeled with the DNA dye Hoechst 33258 and sorted according to DNA content by flow cytometry (**Fig. 2C**). Cells from G_1, S, and G_2–M phases were then recorded for I_h separately. Interestingly, we identified cell-cycle–specific ion activity in 41% cells in S-phase (25 of 63 cells) and 72% in G_2–M (8 of 11 cells) while no activity was seen in the G_1–G_0 cell-cycle phase ($n = 15$; **Fig. 2C**). Moreover, cells in S-G_2–M phases that exhibited I_h had a mean E_m significantly more depolarized than I_h-negative cells (**Fig. 2D**). To corroborate these findings, we analyzed I_h currents by patch-clamp in cells in S-G_2–M phases in primary neurospheres using the FUCCI cell-cycle reporter Gem-AG (26) and again found that cells positive for I_h had a more depolarized membrane potential than cells lacking I_h (**Fig. 2E**). These data demonstrate that HCN channel activity maintains depolarized membrane potential in replicating NSCs.

We next examined the relative HCN2 and HCN3 expression levels over cell-cycle phases (as identified by DNA content) were examined by flow cytometry. Reflecting the I_h activity profile over the cell cycle, HCN2 channel expression increased in the S-G_2–M phases (**Fig. 2F** and **G**; Supplementary Fig. S1A). Moreover, confocal microscopy analyses after sorting cell-cycle phases by flow cytometry, showed increased HCN2 expression and localization to the cell surface in the S and G_2–M phase as compared with G_1 (**Fig. 2H**). In conclusion, the data identify HCN channel-mediated I_h currents to be restricted to S-G_2–M phases of the cell cycle and that it plays a role in depolarizing the membrane potential in NSCs.

HCN channel function is required for sustained spontaneous calcium oscillations

Calcium oscillations and waves have been shown to correlate with cell cycle progression in neural progenitor cells *in vitro* (40, 41) and in the SVZ (42). As we had found that HCN channels control membrane potential in NSCs and that HCN2 channels are calcium permeable, we hypothesized that the HCN channels might play a role in spontaneous calcium oscillations. We therefore performed live-cell time-lapse imaging of NSCs and recorded spontaneous calcium oscillations in the presence or absence of the HCN channel blocker ZD7288. Whereas 83% of the oscillating cells continued to oscillate 15 minutes after vehicle application, only 16% of the cells continued to oscillate after administration of the channel blocker (**Fig. 2I** and **J**). A similar effect was found using the nonspecific HCN channel blocker cesium (**Fig. 2K**) and this effect was reversible as following cesium wash-out, cells resumed oscillations albeit with an altered frequency (**Fig. 2K**). These data suggest that HCN channel activity plays a direct role in maintaining spontaneous calcium oscillations in NSCs.

HCN channels regulate NSC proliferation

To directly test a role for HCN channels in regulating NSC proliferation, primary neurospheres established from SVZ of adult mice, were treated with an HCN channel inhibitor (ZD7288) for four days. This resulted in the formation of smaller neurospheres compared with controls (**Fig. 3A**), supporting a role for HCN channels in NSC proliferation. Treatment of adherent NSCs with ZD7288 for two days at concentrations 0.1–100 μmol/L showed a dose-dependent reduction in cell numbers as measured by an ATP assay (**Fig. 3B**) with an EC_{50} of 1.1 μmol/L. Two additional HCN channel blockers, Zatebradine and cesium, likewise showed a dose-dependent effect on cell numbers (**Fig. 3B**). As expected, HCN channel inhibition by ZD7288 reduced DNA synthesis, as shown by lower EdU incorporation (**Fig. 3C**). Importantly, ZD7288 treatment did not increase the number of apoptotic cells, as no increase in active caspase-3–positive NSCs were observed under these conditions (**Fig. 3D**). These results support the conclusion that pharmacologic inhibition of HCN reduces proliferation of NSC cells. To corroborate the pharmacologic studies, *Hcn2*- and *Hcn3*-targeting shRNA constructs were transduced to adherently cultured NSCs. Both constructs resulted in significantly reduced proliferation compared with control cells as assayed by the number of EdU-incorporating cells (**Fig. 3E**).

The possibility that HCN channels play a role in proliferation in neurogenic zones *in vivo* was tested by administration of ZD7288 (4 mg/kg body weight; i.p.) to 21-day-old mice followed by sacrifice after 2, 24, and 72 hours (**Fig. 3F**). Levels of proliferation were assayed by antibody staining for the G_2–M phase marker phosphorylated Histone-3 (PH3) in the SVZ and SGZ (**Fig. 3G**). No effect on proliferation was detected 2 hours after injection of ZD7288 (**Fig. 3H** and **I**). However, 24 hours after injection the number of G_2–M cells was robustly reduced in both the SVZ and SGZ (**Fig. 3G–I**). An equivalent reduction in proliferation after 24 hours was observed when analyzing the marker for active cell cycling, Ki67, in the SVZ and SGZ (Supplementary Fig. S2A and S2B). Furthermore, reduced DNA synthesis as observed by BrdU incorporation was found in both the SVZ and SGZ 24 hours after ZD7288 administration (Supplementary Fig. S2C and S2D). Interestingly, 72 hours after injection, the number of $PH3^+$ cells had returned to control values in both the SVZ and SGZ (**Fig. 3H** and **I**) suggesting that ZD7288 was efficiently cleared from the niche. In conclusion, the transient inhibitory effect on cell proliferation after HCN channel inhibition *in vivo*, suggested that the cell-cycle arrest was reversible indicative of a temporary state of chemical-induced cell quiescence.

HCN channel antagonism induces quiescence in NSCs

To verify that membrane hyperpolarization by HCN channel inhibition causes induction of quiescence in NSCs also *in vitro*, $Ki67^+$ cells were quantified 24 hours after ZD7288 treatment, which showed reduced number of $Ki67^+$ cells (**Fig. 4A**). Effects on cell-cycle distribution by ZD7288 were analyzed by DNA staining and flow cytometry. This showed an increase in the proportion of cells in G_1–G_0 and a decrease in both S and G_2–M fractions after treatment (**Fig. 4B** and **C**). Together, these findings indicate that HCN channel antagonism limits progression beyond G_1–G_0, and as such causes cell-cycle arrest and quiescence.

Next, we assessed whether the effect on proliferation by HCN channel antagonism was reversible in a drug wash-out experiment. NSCs were cultured for 72 hours in the presence of ZD7288 and were subsequently allowed to recover in inhibitor-free media for 48 hours, followed by EdU pulsing. The percentage of EdU-incorporating cells was fully recovered after wash-out confirming the cells' ability to reenter cell cycling (**Fig. 4D**).

In contrast to actively proliferating and replicating cells, quiescent cells are less vulnerable to cell death by radiation and genotoxic drugs. This resistance can thus be used as a proxy to verify cell quiescence and therefore we tested whether HCN channel inhibition could prevent cell death induced by the genotoxic drug arabinofuranosyl cytidine (Ara-C). NSCs were exposed to Ara-C with or without ZD7288 treatment and analyzed 48 hours later. The number of surviving cells measured by ATP assay was significantly higher after treatment with Ara-C together with ZD7288 as compared with Ara-C treatment alone (**Fig. 4E**). A similar protective effect from Ara-C treatment was found for Cs^+ (Supplementary Fig. S3). In summary, these data further support the induction of a quiescence-like state by HCN channel inhibition.

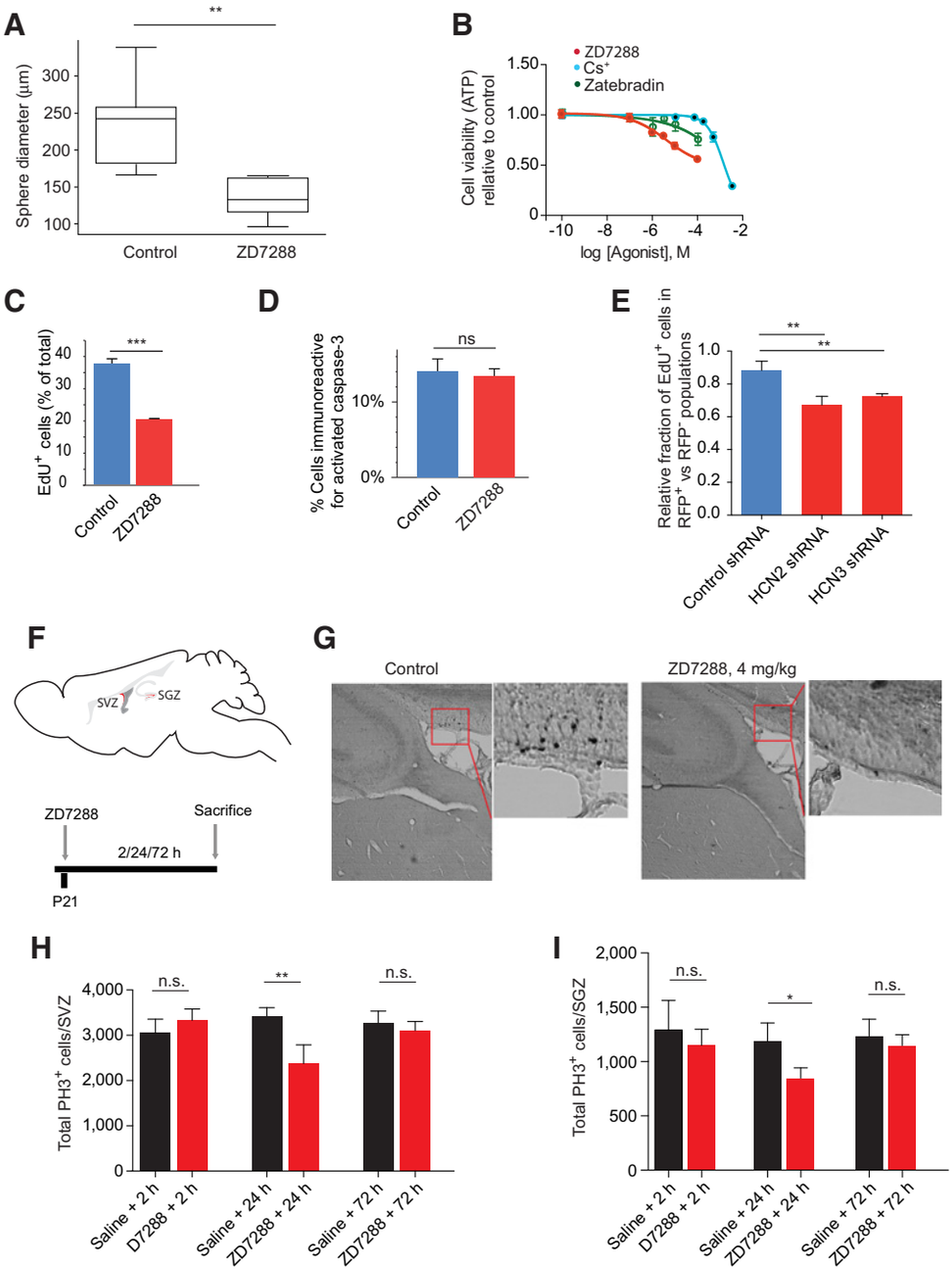

Figure 3.

HCN channels regulate NSC proliferation. **A,** Box plot showing sphere diameters of treated spheres quantified by image analysis (ImageJ). Average sphere diameter was smaller in ZD7288-treated spheres as compared with control ($n = 3$, **, $P \leq 0.01$, Student t test). **B,** Dose–response curve of adherently grown NSCs in relation to control, 48 hours after application of ZD7288, Zatebradine, and CsCl, respectively, as measured by an ATP-based cell assay ($n = 3$ for each treatment, curve fitting by nonlinear regression: log(inhibitor) vs. response, three parameters). **C,** Quantification of percentage of EdU$^+$ cells 24 hours after application of 10 µmol/L ZD7288 and vehicle. A 46% reduction of EdU$^+$ cells was seen after ZD7288 treatment ($n = 3$, ***, $P \leq 0.001$, Student t test). **D,** Quantification of apoptotic cells immunostained for activated caspase-3 showed no significant cell death induced by ZD7288. **E,** Quantification of cell proliferation 48 hours following knockdown of Hcn2 and Hcn3. Stably transduced doxycycline-inducible shRNA constructs targeting Hcn2 and Hcn3 were compared with scrambled control. In addition to the shRNA, all vectors carried a red fluorescent protein (RFP) reporter under the control of the inducible promoter. After induction of shRNA expression and EdU pulsing, proliferation was analyzed by quantifying the fraction of EdU$^+$ cells in RFP$^+$-transduced cells and compared with the fraction of EdU$^+$ cells in the RFP$^-$ population. In contrast to scrambled control, stably transduced shRNAs targeting Hcn2 and Hcn3 both resulted in significantly reduced EdU incorporation ($n = 3$ for each construct, *, $P \leq 0.01$, Student t test). **F,** Assessment of proliferating cells in SVZ and SGZ. **G** and **H,** Quantification of PH3 immunoreactivity 2 hours, 24 hours, and 72 hours after intraperitoneal administration of 4 mg/kg ZD7288 and vehicle in SVZ ($n = 5$ animals). **I,** Identical analysis in SGZ ($n = 5$ animals; n.s. not significant; *, $P \leq 0.05$; **, $P \leq 0.01$, Student t test).

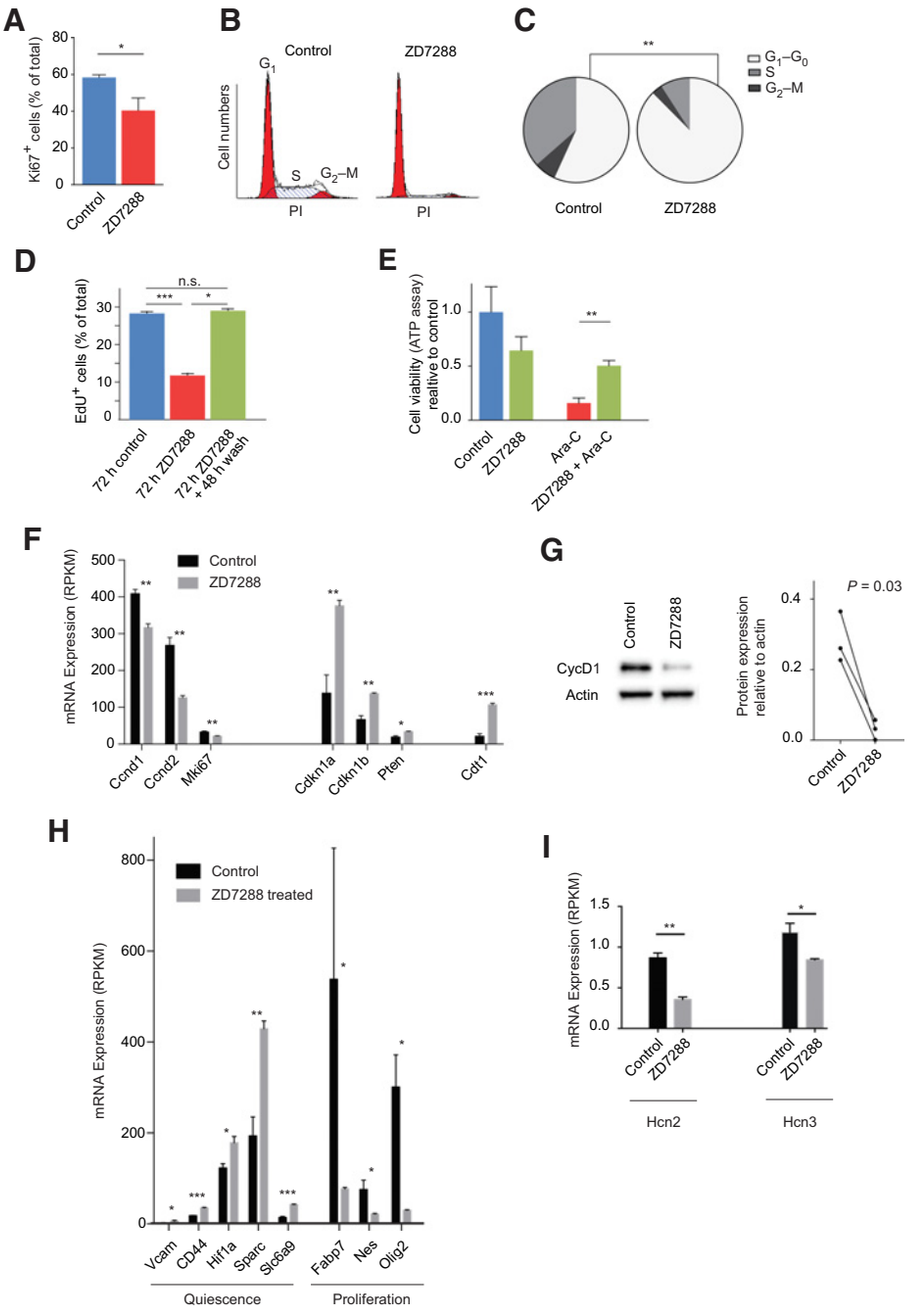

Figure 4.

HCN channel inhibition induces quiescence in NSCs. **A,** Determination of percentage of NSCs in active cell cycling by quantification of percentage of $Ki67^+$ cells. A 31% reduction of $Ki67^+$ cells was seen after ZD7288 (10 μmol/L) treatment as indicative of quiescence ($n = 3$, *, $P \le 0.05$, Student t test). **B** and **C,** Cell-cycle profile of ZD7288-treated and vehicle-treated cells was determined by propidium iodine (PI) staining and flow cytometry. **C,** Pie-chart with relative numbers of cells in each cell-cycle stage showed an accumulation of cells in G_1–G_0 following 24-hour ZD7288 treatment as compared with control ($n = 3$, **, $P \le 0.01$, Student t test). **D,** Quantification of EdU^+ cells following 72-hour treatment with ZD7288 indicated a decreased proliferative level compared with control and returned to control levels 48-hour after wash-out, ($n = 3$, Student t test, not significant, n.s.). **E,** Quantification of cell viability (ATP-based cell assay) following treatment with genotoxic drug (Ara-C, 1 μmol/L) in the presence or absence of ZD7288. Treatment with ZD7288 appeared to protect NSCs from Ara-C effect, indicating induced quiescence (control $n = 3$, Ara-C–treated cells $n = 2$, **, $P \le 0.01$, Student t test). **F,** Expression analysis by RNA sequencing after 24 hours of ZD7288 treatment showed changes in expression of multiple cell-cycle markers ($n = 3$ for controls and $n = 2$ for ZD7288 treatment, *, $P \le 0.05$; **, $P \le 0.01$; ***, $P \le 0.001$, FDR). **G,** Western blot analyses showing expression levels of Cyclin D1 in vehicle-treated and 24-hour ZD7288-treated NSCs. Protein expression levels were quantified relative to β-actin. Cyclin D1 protein expression was reduced following HCN channel inhibition ($n = 3$, Student t test). **H,** Quiescence/proliferation marker expression in the RNA-sequencing data after 24 hours of ZD7288 treatment (control $n = 3$, ZD7288 $n = 2$; *, $P \le 0.05$; **, $P \le 0.01$; ***, $P \le 0.001$, FDR). **I,** HCN channel expression after 24-hour ZD7288 treatment ($n = 3$ for controls and $n = 2$ for ZD7288 treatment; *, $P \le 0.05$; **, $P \le 0.01$, FDR).

Gene expression responses to HCN channel antagonism in NSCs

We comprehensively assessed genome-wide responses to membrane hyperpolarization by HCN channel inhibition in an unbiased manner by performing a transcriptome analysis by RNA sequencing of NSCs (100,000 cells per sample) 24 hours after ZD7288 exposure (Key Resource Table). A significant change in expression of a large number of genes was found (2,845 genes at FDR ≤ 0.01; Key Resource Table; Supplementary Fig. S4A). Further supporting the notion that hyperpolarization by HCN inhibition induces quiescence, several markers of active proliferation were downregulated in ZD7288-treated NSCs, including *Ccnd1*, *Ccnd2*, and *Mki67* while markers of cell-cycle arrest/quiescence were upregulated, including *Cdkn1a* (p21), *Cdkn1b* (p27), and the G_1 phase marker *Cdt1* (**Fig. 4F**). Western blot validated a downregulation of Cyclin D1 after 24 hours of ZD7288 treatment (**Fig. 4G**). The transcriptome analysis further showed that markers of qNSCs were upregulated by HCN channel inhibition (such as *Vcam, CD44* and *Hif1a*) and markers of aNSCs were downregulated (*Fabp7, Nes*, and *Olig2*; **Fig. 4H**; refs. 13, 43, 44). Remarkably, HCN channel expression itself was downregulated by HCN channel block (**Fig. 4I**) identifying HCN channel expression to be selective for actively proliferating NSCs. HCN channel expression and cell proliferation thus appear to be regulated in a reciprocal fashion.

To verify that HCN channel inhibition–induced cell-cycle arrest was not a result of terminal differentiation, the expression of stemness- and differentiation-associated genes was analyzed in the transcriptome data from ZD7288-treated and nontreated cells. No differentiation markers were found to be upregulated, and expression of the multipotency marker *Sox2* was unaltered (Supplementary Fig. S4).

Neuroprotective effect *in vivo* by HCN channel inhibition

Cancer therapy during adolescence can result in long-lasting cognitive impairment (2). This may partly be caused by damage to dividing NSCs in the developing brain primarily in the SGZ in the hippocampus (8). We hypothesized that the drug-induced quiescence we identified in our study would provide a protective effect during cancer therapy, provided that cancer cells maintain sensitivity to genotoxic treatment. We therefore first assessed the expression levels of HCN by RNA sequencing and showed that HCN ion channels were expressed in human fetal NSCs (hfNSCs) as well as in GICs (ref. 45; **Fig. 5A**). The hfNSCs and the GICs were then tested for HCN channel inhibition effects on proliferation by EdU pulsing. While EdU incorporation was decreased in the hfNSCs after ZD7288 treatment, GICs showed no difference in comparison with control (**Fig. 5B**). A larger set of GICs was tested in a dose–response analysis of ZD7288, which in a similar manner showed no effect on cell numbers (**Fig. 5C**). The data therefore suggest that HCN channel activity is a distinctive regulatory feature of normal NSCs that is lost in brain tumor–initiating cells that therefore remain sensitive to chemo- and radiotherapy in the presence of ZD7288.

A selective effect on NSCs with respect to induction of quiescence might be a basis for protecting NSCs during cancer therapy. To test this idea *in vivo*, we next analyzed whether HCN channel inhibition provides protection of NSCs during radiotherapy in a mouse model. ZD7288 (8 mg/kg) was administered (i.p.) to P11 mice and 24 hours later P12 animals were exposed to 2 Gy ionizing radiation (IR) and sacrificed 6 hours later (**Fig. 5D**). ZD7288 treatment resulted in a reduction in pyknotic nuclei in the SGZ as assayed by Nissl nucleic acid staining (**Fig. 5E** and **F**) and a decrease in irradiation-induced apoptosis in SGZ cells as assayed by IHC against activated caspase-3 (**Fig. 5G**). Furthermore, measuring the number of proliferating cells, as measured by IHC against PH3, showed that the number of $PH3^+$ cells in irradiated and ZD7288-treated animals was significantly higher than in irradiated and nontreated animals (**Fig. 5H**) indicating that cells reversibly arrested by ZD7288 had survived radiation and returned to cell cycling at the time of sacrifice. A similar result was found in animals that were BrdU pulsed prior to sacrifice, in which the numbers of $BrdU^+$ cells were higher in irradiated and ZD7288-treated animals in comparison with irradiated and nontreated animals (**Fig. 5I**). In conclusion, these data highlight a divergence in dependence on HCN activity between normal NSCs and malignant GICs and demonstrate that HCN channel inhibition provides a unique therapeutic benefit by protecting NSCs during cancer therapy by radiation and likely also by genotoxic drugs (**Fig. 5J**).

Discussion

Ion channels regulate dynamic alterations in ion homeostasis and membrane potential in control of NSC proliferation. Here we identify HCN as a new component in the channel network in NSCs required to maintain NSCs in the actively proliferating pool. Importantly, the requirement for active HCN channels was unique for normal NSCs in contrast to malignant brain tumor–initiating cells, suggesting a divergence in electrochemical function between normal and malignant cell types. However, further investigations are needed to clarify whether the difference between normal and malignant cells lies in membrane potential or indirectly in pathways downstream of ion fluxes. Interestingly, this divergence provides a cell type–selective target for rescue during cancer treatment by inducing quiescence in NSCs.

Our electrophysiologic recordings revealed that HCN-mediated I_h-currents were restricted to S-G_2–M cell-cycle phases and accompanied elevated membrane potentials. This is in agreement with previously reports showing that cells entering S-phase depolarize (46–49). Furthermore, we found that hyperpolarization via inhibition of HCN channel activity caused NSCs to accumulate in G_1–G_0 and enter a quiescent state, suggesting a function of HCN channels in progression through the G_1–S transition or for reentrance into cell cycling following quiescence.

Our results showed HCN channels to be necessary for spontaneous calcium oscillations. Interestingly, calcium oscillations have previously been shown to be restricted to G_1 to S-phase transition and associated with cell-cycle progression in neuronal (44) and cardiac progenitor cells (45). Our results thus suggest that HCN-mediated currents maintain calcium oscillations necessary for progression through the cell cycle. HCN channels furthermore have a unique property of being activated by hyperpolarization and contributing to electrical feedback loops in membrane potential that may be a driver of calcium oscillations. Interestingly, as HCN2 channels are calcium-permeable (18), this channel could participate directly in calcium oscillations although more detailed investigations are needed to prove this. Taken together, these observations strengthen a mechanistic connection between HCN activity, calcium oscillations, and cell-cycle progression.

In our study, calcium oscillations were blocked by both ZD7288 and Cs^+. While the selectivity of ZD7288 towards HCN channels has been challenged, as T-type VGCC currents are blocked in one study (50), this was at a significantly higher IC_{50} (IC_{50} 1.4 μmol/L for HCN and 40 μmol/L for T-type VGCCs). In our study, we used 10 μmol/L ZD7288 and the VGCC is therefore an unlikely target. Supporting that HCN and not T-type VGCCs are targeted in our study is the fact that the T-type channel blockers niguldipine and mibefradil effectively caused cell death in GICs in our previous study (27). In this study, GICs were resistant to ZD7288 at 10μmol/L excluding block of T-type channels at this concentration.

Our data mining and previous studies show that $GABA_A$ receptors are expressed in qNSCs (51) and reduce proliferation via hyperpolarization of the membrane potential (14, 52). We show that HCN channels and $GABA_A$ receptors are differentially transcriptionally encoded in active and quiescent state respectively to dictate proliferation in NSC in opposite directions (**Fig. 5K**). Noteworthily, both glutamate and GABA-gated receptors control proliferation in cancer cells, including GICs (53, 54). HCN channel activity therefore has a potentially unique function in NSCs. This opens unexpected possibilities when designing neuroprotective strategies that we explored in this study.

Our results provide a foundation for neuroprotection addressing the problem from a different angle than previous studies. These studies utilize lithium administration to alleviate effects from damage on NSCs and have therefore focused on augmenting NSC proliferation after the damaging event (8, 9, 10) aiming to stimulate postdamage repair of the nervous system. In contrast, our study, to our knowledge, is the first to report cell type–specific protection of NSCs during the genotoxic insult itself and may therefore provide a starting point for the development of a new type of protective strategies. Encouragingly, the two strategies can be sequentially

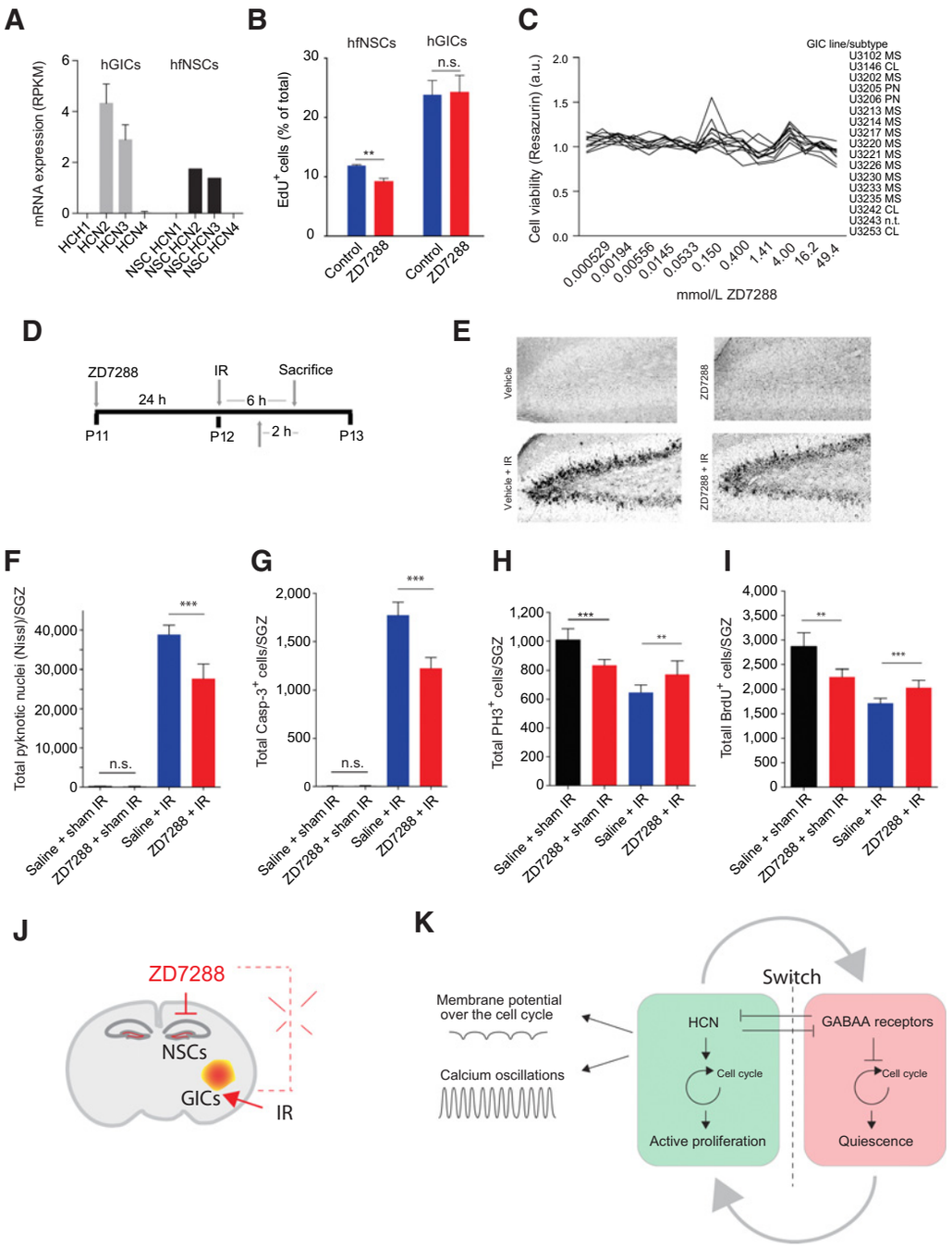

Figure 5.

Cancer cells are insensitive to HCN channel inhibition despite HCN channel expression and HCN channel inhibition protects NSC irradiation–induced cell death. **A,** HCN mRNA isoform expression in hGICs and hfNSCs (RPKM values from RNA sequencing, hGICs $n = 3$, hfNSCs $n = 1$). **B,** Analysis of fraction of EdU^+ cells in hfNSCs and hGICs after application of 24 hours of 10μmol/L ZD7288 (all conditions $n = 3$, except hfNSCs control $n = 2$; **, $P \leq 0.01$, Student t test). **C,** Quantification of cell numbers assaying for viability using resazurin in 17 patient-derived GIC lines after application of 72 hours of ZD7288 [GIC subtypes (55): MS mesenchymal; PN, proneural; CL, classical; n.t., not tested]. **D–I,** Schematic overview of ZD7288 administration (8 mg/kg) in combination with IR (2 Gy) in mice (P11-P12). After IR and ZD7288 treatment, animals were sacrificed and stereologic cell counting was done in sagittal sections of SGZ/hippocampus. **E** and **F,** Nissl staining for pyknotic nuclei in the SGZ after IR with or without ZD7288 administration (number of animals in each condition: $n = 5$, $n = 6$, $n = 9$, $n = 9$, respectively; ***, $P \leq 0.001$, Student t test). **G,** Analysis of apoptosis by immunostaining for cleaved caspase-3 after IR combined with ZD7288 or vehicle administration (animals in each condition: $n = 5$, $n = 6$, $n = 9$, $n = 9$, respectively; ***, $P \leq 0.001$, Student t test). Analysis of proliferation was assayed by immunostaining for PH3 (**H**) and BrdU (**I**; animals in each condition: $n = 5$, $n = 6$, $n = 9$, $n = 9$, respectively; **, $P \leq 0.01$, Student t test). **J,** Proposed therapeutic model for neuroprotection targeting HCN activity. **K,** Schematic of balancing effects on membrane potential by HCN channels and $GABA_A$ receptors shaping proliferative status of NSCs.

administered, first protecting NSCs and then stimulating expansion of intact NSCs to induce repair.

Disclosure of Potential Conflicts of Interest

No potential conflicts of interest were disclosed.

Authors' Contributions

H. Johard: Conceptualization, supervision, investigation, writing-original draft. **A. Omelyanenko:** Investigation, writing-original draft. **G. Fei:** Investigation. **M. Zilberter:** Investigation. **Z. Dave:** Investigation. **R. Abu-Youssef:** Investigation. **L. Schmidt:** Investigation. **A. Harisankar:** Investigation. **C.T. Vincent:** Writing-original draft. **J. Walfridsson:** Supervision. **S. Nelander:** Supervision. **T. Harkany:** Resources, supervision, writing-review and editing. **K. Blomgren:** Resources, supervision. **M. Andäng:** Conceptualization, resources, data curation, supervision, funding acquisition, writing-original draft, project administration, writing-review and editing.

Acknowledgments

We thank HGCC at Uppsala University for providing GICs and Peter Dirks at the University of Toronto for providing hfNSCs. We also thank Sten Linnarsson for assistance on RNA sequencing and Anders Mutvei and Eva Hedlund for editing of the manuscript. The study was supported by grants from the Swedish Research Council (grant no. 2014-03035, to M. Andäng; K2013-62X-14250-12-3 and 2019-01684, to K. Blomgren), Swedish Cancer Foundation (CAN 2018/340, to M. Andäng; CAN 2017/586, to K. Blomgren), Swedish Childhood Cancer Foundation (PR2018-0094, to M. Andäng; PR2015-0157 and PR2018-0158, to K. Blomgren), Märta och Gunnar V. Philipson Foundation and Stockholm County Council (ALF projects, to K. Blomgren), the Grant Agency of Masaryk University (GAMU)–MUNI/G/1391, the Grant Agency of the Czech Republic (GA15-20818S, GA15-21789S), and European Regional Development Fund-Project MSCAfellow@MUNI (CZ.02.2.69/0.0/0.0/17 050/0008496; to M. Andäng).

The costs of publication of this article were defrayed in part by the payment of page charges. This article must therefore be hereby marked *advertisement* in accordance with 18 U.S.C. Section 1734 solely to indicate this fact.

Received March 30, 2020; revised June 9, 2020; accepted July 10, 2020; published first July 14, 2020.

References

1. Galligan AJ. Childhood cancer survivorship and long-term outcomes. Adv Pediatr 2017;64:133–69.
2. Makale MT, McDonald CR, Hattangadi-Gluth JA, Kesari S. Mechanisms of radiotherapy-associated cognitive disability in patients with brain tumours. Nat Rev Neurol 2017;13:52–64.
3. Lima SMA, Gomes-Leal W. Neurogenesis in the hippocampus of adult humans: controversy "fixed" at last. Neural Regen Res 2019;14:1917–8.
4. Abdul Kadir L, Stacey M, Barrett-Jolley R. Emerging roles of the membrane potential: action beyond the action potential. Front Physiol 2018;9:1661.
5. Eriksson PS, Perfilieva E, Bjork-Eriksson T, Alborn AM, Nordborg C, Peterson DA, et al. Neurogenesis in the adult human hippocampus. Nat Med 1998;4:1313–7.
6. Ernst A, Alkass K, Bernard S, Salehpour M, Perl S, Tisdale J, et al. Neurogenesis in the striatum of the adult human brain. Cell 2014;156:1072–83.
7. Spalding KL, Bergmann O, Alkass K, Bernard S, Salehpour M, Huttner HB, et al. Dynamics of hippocampal neurogenesis in adult humans. Cell 2013;153:1219–27.
8. Michaelidesova A, Konirova J, Bartunek P, Zikova M. Effects of radiation therapy on neural stem cells. Genes 2019;10:640.
9. Huo K, Sun Y, Li H, Du X, Wang X, Karlsson N, et al. Lithium reduced neural progenitor apoptosis in the hippocampus and ameliorated functional deficits after irradiation to the immature mouse brain. Mol Cell Neurosci 2012;51:32–42.
10. Zanni G, Di Martino E, Omelyanenko A, Andang M, Delle U, Elmroth K, et al. Lithium increases proliferation of hippocampal neural stem/progenitor cells and rescues irradiation-induced cell cycle arrest in vitro. Oncotarget 2015;6:37083–97.
11. Morales AV, Mira H. Adult neural stem cells: born to last. Front Cell Dev Biol 2019;7:96.
12. Mira H, Andreu Z, Suh H, Lie DC, Jessberger S, Consiglio A, et al. Signaling through BMPR-IA regulates quiescence and long-term activity of neural stem cells in the adult hippocampus. Cell Stem Cell 2010;7:78–89.
13. Mazumdar J, O'Brien WT, Johnson RS, LaManna JC, Chavez JC, Klein PS, et al. O2 regulates stem cells through Wnt/beta-catenin signalling. Nat Cell Biol 2010;12:1007–13.
14. Yeh CY, Asrican B, Moss J, Quintanilla LJ, He T, Mao X, et al. Mossy cells control adult neural stem cell quiescence and maintenance through a dynamic balance between direct and indirect pathways. Neuron 2018;99:493–510.
15. Yang M, Brackenbury WJ. Membrane potential and cancer progression. Front Physiol 2013;4:185.
16. Lau YT, Wong CK, Luo J, Leung LH, Tsang PF, Bian ZX, et al. Effects of hyperpolarization-activated cyclic nucleotide-gated (HCN) channel blockers on the proliferation and cell cycle progression of embryonic stem cells. Pflugers Arch 2011;461:191–202.
17. Omelyanenko A, Sekyrova P, Andang M, Andäng M. ZD7288, a blocker of the HCN channel family, increases doubling time of mouse embryonic stem cells and modulates differentiation outcomes in a context-dependent manner. Springerplus. SpringerOpen; 2016;5:1–10.
18. Michels G, Brandt MC, Zagidullin N, Khan IF, Larbig R, Van Aaken S, et al. Direct evidence for calcium conductance of hyperpolarization-activated cyclic nucleotide-gated channels and human native If at physiological calcium concentrations. Cardiovasc Res 2008;78:466–75.
19. Biel M, Schneider A, Wahl C. Cardiac HCN channels: structure, function, and modulation. Trends Cardiovasc Med 2002;12:206–12.
20. Shah MM. Recording hyperpolarization-activated cyclic nucleotide-gated channel currents (Ih) in neurons. Cold Spring Harb Protoc 2016;2016.
21. Atkinson SE, Maywood ES, Chesham JE, Wozny C, Colwell CS, Hastings MH, et al. Cyclic AMP signaling control of action potential firing rate and molecular circadian pacemaking in the suprachiasmatic nucleus. J Biol Rhythm 2011;26:210–20.
22. O'Neill JS, Maywood ES, Chesham JE, Takahashi JS, Hastings MH. cAMP-dependent signaling as a core component of the mammalian circadian pacemaker. Science 2008;320:949–53.
23. Zhuo L, Sun B, Zhang CL, Fine A, Chiu SY, Messing A. Live astrocytes visualized by green fluorescent protein in transgenic mice. Dev Biol 1997;187:36–42.
24. Fernando RN, Eleuteri B, Abdelhady S, Nussenzweig A, Andang M, Ernfors P. Cell cycle restriction by histone H2AX limits proliferation of adult neural stem cells. Proc Natl Acad Sci U S A 2011;108:5837–42.
25. Conti L, Pollard SM, Gorba T, Reitano E, Toselli M, Biella G, et al. Niche-independent symmetrical self-renewal of a mammalian tissue stem cell. PLoS Biol 2005;3:e283.
26. Sakaue-Sawano A, Kurokawa H, Morimura T, Hanyu A, Hama H, Osawa H, et al. Visualizing spatiotemporal dynamics of multicellular cell-cycle progression. Cell 2008;132:487–98.
27. Niklasson M, Maddalo G, Sramkova Z, Mutlu E, Wee S, Sekyrova P, et al. Membrane-depolarizing channel blockers induce selective glioma cell death by impairing nutrient transport and unfolded Protein/Amino acid responses. Cancer Res 2017;77:1741–52.
28. Islam S, Kjallquist U, Moliner A, Zajac P, Fan JB, Lonnerberg P, et al. Characterization of the single-cell transcriptional landscape by highly multiplex RNA-seq. Genome Res 2011;21:1160–7.
29. Langmead B, Trapnell C, Pop M, Salzberg SL. Ultrafast and memory-efficient alignment of short DNA sequences to the human genome. Genome Biol 2009;10:R25.
30. Mortazavi A, Williams BA, McCue K, Schaeffer L, Wold B. Mapping and quantifying mammalian transcriptomes by RNA-Seq. Nat Methods 2008;5:621–8.
31. Chang K, Marran K, Valentine A, Hannon GJ. Creating an miR30-based shRNA vector. Cold Spring Harb Protoc 2013;2013:631–5.
32. Meerbrey KL, Hu G, Kessler JD, Roarty K, Li MZ, Fang JE, et al. The pINDUCER lentiviral toolkit for inducible RNA interference *in vitro* and *in vivo*. Proc Natl Acad Sci U S A 2011;108:3665–70.

33. Zanni G, Goto S, Fragopoulou AF, Gaudenzi G, Naidoo V, Di Martino E, et al. Lithium treatment reverses irradiation-induced changes in rodent neural progenitors and rescues cognition. Mol Psychiatry 2019.
34. Xie Y, Bergstrom T, Jiang Y, Johansson P, Marinescu VD, Lindberg N, et al. The Human glioblastoma cell culture resource: validated cell models representing all molecular subtypes. EBioMedicine 2015;2:1351–63.
35. Pollard SM, Yoshikawa K, Clarke ID, Danovi D, Stricker S, Russell R, et al. Glioma stem cell lines expanded in adherent culture have tumor-specific phenotypes and are suitable for chemical and genetic screens. Cell Stem Cell 2009;4:568–80.
36. Bostrom M, Kalm M, Karlsson N, Hellstrom Erkenstam N, Blomgren K. Irradiation to the young mouse brain caused long-term, progressive depletion of neurogenesis but did not disrupt the neurovascular niche. J Cereb Blood Flow Metab 2013;33:935–43.
37. Codega P, Silva-Vargas V, Paul A, Maldonado-Soto AR, Deleo AM, Pastrana E, et al. Prospective identification and purification of quiescent adult neural stem cells from their in vivo niche. Neuron 2014;82:545–59.
38. Notomi T, Shigemoto R. Immunohistochemical localization of Ih channel subunits, HCN1–4, in the rat brain. J Comp Neurol 2004;471:241–76.
39. Pastrana E, Cheng LC, Doetsch F. Simultaneous prospective purification of adult subventricular zone neural stem cells and their progeny. Proc Natl Acad Sci U S A 2009;106:6387–92.
40. Resende RR, Adhikari A, da Costa JL, Lorencon E, Ladeira MS, Guatimosim S, et al. Influence of spontaneous calcium events on cell-cycle progression in embryonal carcinoma and adult stem cells. Biochim Biophys Acta 2010;1803:246–60.
41. Ferreira-Martins J, Rondon-Clavo C, Tugal D, Korn JA, Rizzi R, Padin-Iruegas ME, et al. Spontaneous calcium oscillations regulate human cardiac progenitor cell growth. Circ Res 2009;105:764–74.
42. Weissman TA, Riquelme PA, Ivic L, Flint AC, Kriegstein AR. Calcium waves propagate through radial glial cells and modulate proliferation in the developing neocortex. Neuron 2004;43:647–61.
43. Basak O, Krieger TG, Muraro MJ, Wiebrands K, Stange DE, Frias-Aldeguer J, et al. Troy+ brain stem cells cycle through quiescence and regulate their number by sensing niche occupancy. Proc Natl Acad Sci U S A 2018;115:E610–9.
44. Su W, Foster SC, Xing R, Feistel K, Olsen RH, Acevedo SF, et al. CD44 transmembrane receptor and hyaluronan regulate adult hippocampal neural stem cell quiescence and differentiation. J Biol Chem 2017;292:4434–45.
45. Wee S, Niklasson M, Marinescu VD, Segerman A, Schmidt L, Hermansson A, et al. Selective calcium sensitivity in immature glioma cancer stem cells. PLoS One 2014;9:e115698.
46. MacFarlane SN, Sontheimer H. Changes in ion channel expression accompany cell cycle progression of spinal cord astrocytes. Glia 2000;30:39–48.
47. Yasuda T, Bartlett PF, Adams DJ. K(ir) and K(v) channels regulate electrical properties and proliferation of adult neural precursor cells. Mol Cell Neurosci 2008;37:284–97.
48. Sundelacruz S, Levin M, Kaplan DL. Role of membrane potential in the regulation of cell proliferation and differentiation. Stem Cell Rev 2009;5:231–46.
49. Urrego D, Tomczak AP, Zahed F, Stuhmer W, Pardo LA. Potassium channels in cell cycle and cell proliferation. Philos Trans R Soc L B Biol Sci 2014;369:20130094.
50. Sánchez-Alonso JL, Halliwell J V, Colino A. ZD 7288 inhibits T-type calcium current in rat hippocampal pyramidal cells. Neurosci Lett 2008;439:275–80.
51. Daynac M, Chicheportiche A, Pineda JR, Gauthier LR, Boussin FD, Mouthon MA. Quiescent neural stem cells exit dormancy upon alteration of GABAAR signaling following radiation damage. Stem Cell Res 2013;11:516–28.
52. Andang M, Hjerling-Leffler J, Moliner A, Lundgren TK, Castelo-Branco G, Nanou E, et al. Histone H2AX-dependent GABA(A) receptor regulation of stem cell proliferation. Nature 2008;451:460–4.
53. Blanchart A, Fernando R, Häring M, Assaife-Lopes N, Romanov RA, Andäng M, et al. Endogenous GAB AA receptor activity suppresses glioma growth. Oncogene 2017;36:777–86.
54. Venkatesh HS, Morishita W, Geraghty AC, Silverbush D, Gillespie SM, Arzt M, et al. Electrical and synaptic integration of glioma into neural circuits. Nature 2019;573:539–45.
55. Wang Q, Hu B, Hu X, Kim H, Squatrito M, Scarpace L, et al. Tumor evolution of glioma-intrinsic gene expression subtypes associates with immunological changes in the microenvironment. Cancer Cell 2017;32:42–56.